Research Article | Vol. 30, No. 23 / 7 Nov 2022 / Optics Express 41219
Optics EXPRESS

Continuous-wave Tm:YLF laser with ultrabroad tuning (1772-2145 nm)

UMIT DEMIRBAS,[1,2,*] JELTO THESINGA,[1] ERSEN BEYATLI,[3] MARTIN KELLERT,[1] MIKHAIL PERGAMENT,[1] AND FRANZ X. KÄRTNER[1,4,5]

[1]Center for Free-Electron Laser Science CFEL, Deutsches Elektronen-Synchrotron DESY, Notkestr. 85, 22607 Hamburg, Germany
[2]Laser Technology Laboratory, Antalya Bilim University, 07190 Dosemealti, Antalya, Turkey
[3]Department of Electrical-Electronics Engineering, Recep Tayyip Erdogan University, Rize, Turkey
[4]Physics Department, University of Hamburg, Luruper Chaussee 149, 22761 Hamburg, Germany
[5]The Hamburg Centre for Ultrafast Imaging, Luruper Chaussee 149, 22761 Hamburg, Germany
*uemit.demirbas@cfel.de

Abstract: We report detailed experimental data aiming for rigorous investigation of Tm:YLF laser performance, especially with a focus on tuning behavior. Continuous-wave (cw) lasing performance of Tm:YLF crystals with thulium dopings in the 2-6% range is investigated under diode and Ti:Sapphire pumping at 792 nm and 780 nm, respectively. While employing the c-axis, we have achieved cw lasing thresholds below 20 mW, laser output power up to 1.42 W, and laser slope efficiencies as high as 70% with respect to absorbed pump power. The passive loss of the Tm:YLF crystal is estimated to be as low as 0.05% per cm, corresponding to a crystal figure of merit above 10000. Via employing this low-loss crystal and a 2-mm thick off-surface optical axis birefringent filter (BRF) with strong sideband rejection, a record cw tuning range covering the 1772-2145 nm interval is demonstrated (except a small gap between 1801-1815nm region). Detailed lifetime and emission cross section measurements have been performed to explain the observed performance, and strategies for further performance enhancement are discussed.

1. Introduction

Yb-based laser systems working around 1 µm region have seen great progress over the last decades, and many high average/peak power ultrafast oscillator/amplifier systems have been developed and are in use in different fields [1–3]. We are also observing a similar interest towards 2 µm laser/amplifier systems based on Tm and Ho solid state gain media [4–8]. As an example, Lawrence Livermore National Laboratory is developing a 1.9 µm Tm:YLF based amplifier for the EuPRAXIA project for laser wakefield acceleration application [9], and Tm:YLF is chosen due to its high energy storage and extraction capabilities [10]. Tm:YLF further possesses a weak thermal lensing [11–13], smaller quantum defect, naturally polarized output, near-unity quantum efficiency [14], and broad emission spectrum, making it an interesting candidate for 2 µm laser research [15].

Tm-based systems, including Tm:YLF, are usually excited using mature high power (multi kW) laser diodes around 800 nm via the $^3H_6 \rightarrow {}^3H_4$ transition (Fig. 1). The material could then be used for broadband lasing around 1.9 µm and 2.3 µm spectral regions via $^3F_4 \rightarrow {}^3H_6$ and $^3H_4 \rightarrow {}^3H_5$ transitions, respectively. Tuning behavior of the 2.3 µm transition of Tm:YLF is investigated by Pinto et al. in 1994, where broadly tunable cw operation in the 2200-2460 nm range with up to 200 mW output power was achieved using a 1.5% doped Tm:YLF crystal [16]. Note that, lasing around 2.3 µm could only be achieved with samples with low Tm-doping (less than 2% [17]), as the cross-relaxation process reduces the fluorescence lifetime of the $^3H_4$ level in highly doped samples [18]. The 2.3 µm lasing action is also not self-terminating [19], since the metastable $^3F_4$

#471288 https://doi.org/10.1364/OE.471288
Journal © 2022 Received 21 Jul 2022; revised 20 Sep 2022; accepted 20 Sep 2022; published 25 Oct 2022

Optics EXPRESS

level prevents the ions to return back to the ground state (population trapping effect [20]). As a result, the laser efficiency obtained in 2.3 μm lasing of Tm:YLF is limited to 47% level [19] and the output powers obtained so far is at 1 W level [18–22].

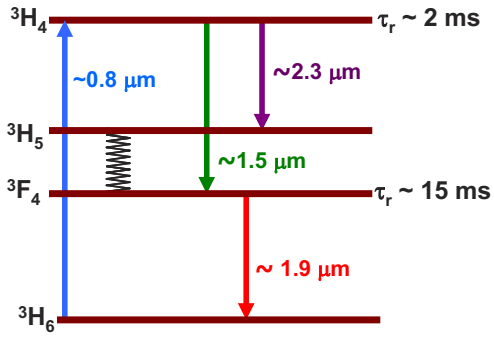

Fig. 1. Simplified energy level diagram of Tm^{+3} ions in $YLiF_4$(YLF).

The cross-relaxation process, which limits the lasing performance around 2.3 μm, enables efficient 1.9 μm lasing in highly Tm-doped samples [23–31], as the process creates an extra inverted ion at the $^3F_4$ level (and hence also known as two-for-one process [16,32]). In 2006, via optimization of the thulium doping level and the geometry of the gain medium, So et al. achieved up to 70 W of output power around 1.9 μm at 44% slope efficiency, from a 2% Tm-doped YLF slab crystal [15,26]. In 2012, Strauss et al. reported a slab Tm:YLF laser employing a 2.5% Tm:YLF crystal with 80 W output power at 1890nm [33]. In 2013, Li et al. achieved 200 W output power from an innoslab Tm:YLF laser using a 2.5%-doped sample, with up to 52% slope efficiency [25]. Recently, Tamer at al. obtained 20 ns pulses with 3.88 J energy and millisecond pulses with 38.1 J energy from a Tm:YLF amplifier system operating at 1 Hz [10].

To investigate the tuning performance of the 1.9 μm transition, in 1997, Ketteridge et al. explored laser operation in cryogenically cooled Tm:YLF, and achieved tuning in the 1840-1890nm (E//c) and 1875-1930nm (E//a) ranges with up to 7 W output power using an intracavity quartz birefringent filter (BRF) [34]. Room-temperature tuning of Tm:YLF is studied in 2007, where Dergachev et al. attained tuning in the 1905-2067nm interval using a BRF with output powers exceeding 5 W (E//c configuration) [28,35]. In 2008, the tuning limit is extended towards shorter wavelengths down to 1835nm with powers approaching 3 W level (E//c configuration, overall tuning: 1835-2010nm) [36]. Recently, the long wavelength tuning edge is stretched up to 2096nm (overall tuning range: 2018-2096), using a 0.13 mm thick intracavity YAG etalon for tuning (E//c configuration) [37].

In this work, we have investigated cw lasing performance of Tm:YLF laser gain media in detail near 1.9 μm (for the $^3F_4 \rightarrow {}^3H_6$ transition), with a focus on cw tuning behavior. We have employed the higher gain E//c axis configuration in our study and lasing performance of Tm:YLF crystals with thulium doping levels of 2, 3 and 6% have been comparatively investigated both under diode (792 nm) and Ti:Sapphire laser (780 nm) pumping. We have shown that the Tm:YLF crystals that are employed in this study possesses a loss of only around 0.05% per cm, corresponding to a figure of merit above 10000. By employing these low-loss crystals, we have achieved lasing thresholds below 20 mW, and laser slope efficiencies as high as 70% (with respect to absorbed pump power). Via usage of a specially-designed birefringent filter optimized for side-band rejection (an off-surface optical axis BRF with a diving angle of 25° [38–41]), we have shown tuning in the 1772-2145 nm range (373 nm overall tuning). The tuning range could be covered smoothly except a small gap in the 1801-1815nm region. To our knowledge, the demonstrated tuning range in this study extends the earlier Tm:YLF tuning reports in literature considerably on

Optics EXPRESS

both short and long wavelength sides (overall tuning range of earlier studies covers 1831-2096nm region, 265 nm tuning) [28,36,37,42–45]. We have further performed detailed lifetime and emission cross section measurements to support our lasing data. The lifetime measurements suggest that even the highly-doped Tm:YLF sample we have used possesses quite low level of impurities, in accordance with the loss measurements. Emission measurements and gain cross section estimates are used to explain the observed tuning behavior. We also provide a detailed discussion on advantages of off-surface optical axis birefringent plates compared to regular on-surface optical axis filters in tuning of Tm:YLF systems.

The paper is organized as follows: Sect. 2 introduces the experimental methodology. In Sect. 3, we present spectroscopic measurement results. Cw lasing and tuning results are presented in Sections 4 and 5 respectively. A detailed Appendix section discusses the advantages of off-surface optical axis birefringent filters for tuning.

2. Experimental setup

Figure 2 (a) shows a schematic of the Tm:YLF laser we have employed while investigating the laser performance. The system is either pumped by a low-cost single emitter multimode diode (MMD) or a Ti:Sapphire laser. The multimode diode (LDX-3315-792-C from LDX Optronics Inc.) has an emitter size of 150 µm, and provides up to 4 W of output power around 792 nm (diode current: 3.6 A, diode voltage: 1.8 V, diode efficiency:~60%). The diode spectrum has a full-width half maximum (FWHM) of around 1.75 nm. The home-build Ti:Sapphire laser provides 2 W of output power around 780 nm and has a spectral width of around 0.25 nm. A flip mirror enables usage of the MMD or the Ti:Sapphire laser as the pump source. Both of the pump sources are linearly polarized, and the E//c axis of Tm:YLF crystal with stronger absorption is employed for pumping (incident pump light is TM polarized).

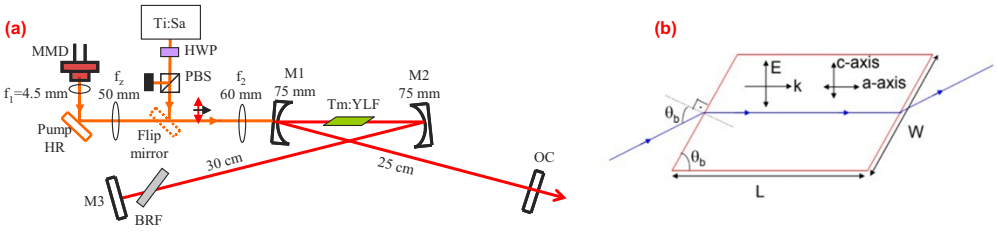

Fig. 2. (a) A simple schematic of the continuous-wave Tm:YLF laser. The system is either pumped by a 792 nm single-emitter multimode diode (MMD) or a 780 nm Ti:Sapphire (Ti:Sa) laser. OC: Output coupler, BRF: Birefringent filter, HWP: Half-wave plate, PBS: Polarizing beam splitter cube. (b) Top view of Brewster-Brewster cut Tm:YLF crystals optimized for lasing in E//c axis. Path of a TM (p) polarized intracavity laser beam is shown in blue.

The MMD output beam is highly asymmetric and divergent. Hence, a 4.5 mm focal length aspheric lens (f_1) is first used to collimate its output. A cylindrical lens (f_z) with a focal length of 50 mm is employed to minimize the diode beam astigmatism. An achromatic doublet with a focal length of 60 mm (f_2) is utilized to focus the pump beam to a waist of around 35 µm x 150 µm inside the laser crystal. For the Ti:Sapphire pump, the beam waist inside the crystal is estimated to be around 40 µm x 80 µm. Three commercial (Optogama) Brewster-Brewster cut Tm:YLF crystals with various Tm-doping are employed in the laser experiments: (i) a 2% Tm-doped YLF with a length of 10 mm, (ii) a 3% Tm-doped YLF with a length of 7 mm, and (iii) a 6% Tm-doped YLF crystal with a length of 4 mm. All the crystals have a width (W) of 6-mm and a thickness of 2 mm. The crystals are a-cut and the Brewster cut surfaces are optimized for lasing

Optics EXPRESS

in E//c configuration (Fig. 2 (b)). The crystals are mounted with indium foil in a copper holder under water cooling at 15 °C.

The crystal lengths are chosen to obtain similar absorption levels at all samples. The estimated small signal absorption of the 2%, 3% and 6% doped crystals for TM polarized pump light at 780 nm are 85.9%, 87.2% and 90.5%, respectively. For the TM polarized pump light at 792 nm, the estimated small signal absorption reduces to 78.6%, 80.2% and 84.2%, respectively. On the other hand, due to the small pump saturation intensity of Tm:YLF (2.5 kW/cm^2), we have observed strong decrease of absorption at high pump power levels (in non lasing conditions). As an example, the measured absorption of the 2% Tm-doped YLF sample decreased from around 78.7% to 58.1% at an incident pump power of 3.75 W (measured with the 972 nm diode). While lasing, as the intracavity circulating laser beam balances the pump saturation via stimulated emission, the absorption of the crystal could be kept in the 73-75% range. In our all measurements, we have measured incident and transmitted pump powers carefully, to correctly account for the absorption state of the crystals. Also, we will report all of our results with respect to absorbed pump power, as the absorption of the crystal heavily depends on pump intensity on the sample as well as lasing conditions.

A standard X-type resonator is used for the laser experiments. The laser cavity consisted of two curved high reflector mirrors, each with a radius of curvature of 75 mm (M1 and M2), a flat high reflector (M3), and a flat OC. The arm lengths for the high-reflector and OC end are 30 cm and 25 cm respectively, resulting in a beam waist of ~40 µm x 60 µm inside the crystal. The cavity high-reflectors (M1-M3) have reflective coatings covering the 1785-2155 nm spectral region with a reflectivity above 99.9% and anti-reflection band covering the 650-850 nm range (R < 7%). The mirrors M1-M2 are used around an incidence angle of around 10°, and as a result the coating range specified above is expected to shift slightly towards shorter wavelengths. Note that, due to the presence of horizontally placed Brewster cut surfaces inside the cavity, the output of the laser is TM (p) polarized in most cases. On the other hand, in a few of the tuning experiments, when the laser wavelength is pushed below 1785nm, the laser also worked in a mixed polarization state. We believe that, this is because the coating range of the cavity reflectors (1785-2155 nm), which is specified for unpolarized light, is actually slightly broader for TE (s) polarized light, and to minimize losses the laser prefers to operate in a mixed polarization state for wavelength below 1785nm (this will be discussed in more detail while presenting the tuning results).Eight different output couplers with transmission ranging from 0.2% to 25% are used in the experiments to carefully scan the operation range of the lasers. The 0.2%, 0.5%, 1.5%, 3% and 5% transmitting output couplers have a specified working range of 1800-2300 nm, whereas the 10%, 15% and 20% output couplers have coatings optimized for 1820-2050nm interval.

A 2-mm thick off-surface optical axis crystal quartz birefringent filter (BRF) with a diving angle of 25° is inserted at Brewster's angle near the high reflector for smooth tuning of laser wavelength [39]. Compared to a regular on-surface optical axis BRF, the off-surface optical axis BRF employed in this study provides a much stronger sideband rejection, enabling record tuning ranges. Detailed information on the properties of this BRF will be presented in the Appendix section.

We have performed lifetime and emission measurements to help us better understand the measured laser performance. During fluorescence lifetime measurements (Fig. 3 (a)), Tm:YLF crystals are excited while running the MMD diode in pulsed mode: square shaped pulses with 1-50 ms length with 4 W peak power at a repetition rate of 1 Hz (maximum average incident power: 0.2 W). The fluorescence decay signal is measured at 90° with respect to the direction of excitation beam, and a 1000 nm high-pass filter (Thorlabs, FELH1000) is implemented to cut out scattered pump signal. The $^3H_4$ level fluorescence lifetime is measured by monitoring the emission around 1500 nm via a free-space Ge detector (Thorlabs, DET30B) with a 650 ns rise time for 50 ohm termination (sub-20 µs response time with 5 k ohm termination). The $^3F_4$ level

Optics EXPRESS

fluorescence lifetime is measured using an InGaAs detector (Thorlabs, DET10D2) with 25 ns rise time for 50 ohm termination and 30 µs response time under 100 k ohm termination. Pinholes with diameters between 50 µm and 2 mm are used for the estimation of radiation-trapping free lifetimes.

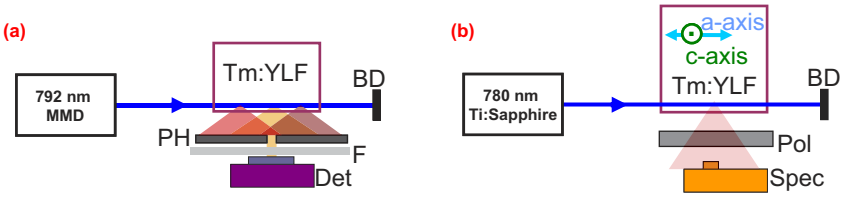

Fig. 3. A simplified schematic of (a) fluorescence lifetime and (b) emission cross section measurements., Det: Detector, F:Filter, PH: Pinhole, Pol: Polarizer, BD: beam dump.

The emission spectra are measured similarly at a 90° angle while exciting the Tm:YLF sample with the Ti:Sapphire laser, using a formalism recently discussed in detail in [46]. A rather small excitation beam size of around 100 µm is used in emission measurements, and the crystal is excited from its edge to minimize self-absorption effects (Fig. 3 (b)). For the emission measurement, a 2.5% Tm-doped rectangular sample with a length of 10 mm and an aperture of 6×6 mm^2 is used to enable easier access to E//a and E//c axes emission. A thin film linear polarizer covering the 1000-3000 nm region (Thorlabs LPNIRA100-MP2) is employed for selecting the fluorescence emission in the relevant axis. The emission is imaged into a low OH silica multimode fiber with a core diameter of 200 µm using a 4 cm focal length uncoated lens. An optical spectrum analyzer (Yokogawa AQ6376) with a spectral resolution of 0.1 nm in the 1500-3400 nm range is used for recording the fluorescence spectra (effective resolution with a 200 µm core fiber is 1 nm, which is adequate for emission data at room-temperature). The spectrometer is purged with nitrogen gas to prevent the influence of air absorption on emission spectra. The emission cross section ($\sigma_e(\lambda)$) is calculated from the measured emission intensities in E//a and E//c axes, using the modified Füchtbauer–Ladenburg formula [47–49]. The room-temperature radiative lifetime of the $^3F_4$ level is taken as 15.25 ms in the emission cross section calculations (see lifetime measurements). McCumber relation is used to estimate absorption cross section $\sigma_a(\lambda)$ from the measured emission cross section via [50–53]:

$$\sigma_a(\lambda) = \frac{Z_u}{Z_l}\sigma_e(\lambda) Exp\left(\frac{\frac{hc}{\lambda} - E_{zl}}{kT}\right) \tag{1}$$

where T is the temperature in Kelvin, h is the Planck constant, k is the Boltzmann constant, c is the speed of light in vacuum, E_{zl} is the energy of the zero phonon line transition (5598 cm^{-1}, 1786.35 nm in vacuum), Z_u (Z_l) is the partition function of the upper (lower) laser manifolds. At room temperature (300 K), Z_u and Z_l has values of 3.4326 and 5.2074, respectively. The effective gain cross section (GCS) spectra ($\sigma_g(\lambda,T)$) of Tm:YLF is estimated using:

$$\sigma_g(\lambda) = \beta\sigma_e(\lambda) - (1-\beta)\sigma_a(\lambda) \tag{2}$$

where β is the fractional population inversion level.

3. Spectroscopic measurements

3.1. Fluorescence lifetime measurements

In this section we will present our fluorescence lifetime measurements. We start with Fig. 4 which shows the measured variation of $^3F^4$ level fluorescence lifetime with pinhole diameter

Optics EXPRESS

for the different Tm:YLF samples at hand. Using a linear fit to the measured data, we have estimated intrinsic (radiation trapping free) fluorescence lifetime of the $^3F_4$ level as 15.25 ms, 16.7 ms, 15.8 ms, 17 ms and 16.3 ms for the 0.5%, 2%, 2.5%, 3% and 6% Tm-doped YLF crystals, respectively. We believe that, the slightly larger estimate for the intrinsic fluorescence lifetime for the crystal with higher doping (15.25 ms with 0.5% doping versus 17 ms for 3% doping), might be due to the remaining effect of radiation trapping, which could not be fully eliminated due to high doping of the samples. In our work, we have taken the radiative lifetime of $^3F_4$ level as 15.25 ms for the calculation of the emission cross section spectra (a value in good agreement with literature [54–56]).

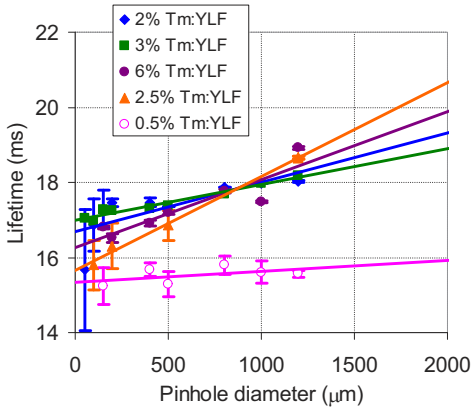

Fig. 4. Measured variation of $^3F_4$ level fluorescence lifetime with pinhole aperture diameter for the 0.5, 2, 2.5, 3 and 6% Tm-doped YLF crystals at room temperature.

Figure 5 (a) shows the variation of reported $^3F_4$ level lifetimes with thulium doping in literature. The results of this work are also included (indicated by blue markers). There is a rather large fluctuation in the reported fluorescence lifetimes of $^3F_4$ level of Tm:YLF in literature [54–67]. In previous literature, the shortening of the $^3F_4$ fluorescence lifetime is attributed to energy-migration to impurities [54,57] (OH^- groups or other rare earth ions [57,68]). Since samples with higher thulium doping usually contain higher amount of impurities, the fluorescence lifetime of $^3F_4$ level tends to be lower in highly Tm-doped samples. Moreover, as the sample quality also depends on care in growth conditions, different growth efforts results in different amount of impurities, which we believe creates the large amount of fluctuation in Fig. 5 (a).

We see from Fig. 5 (a) that, in general, our $^3F_4$ level lifetime measurements for the 0.5%, 2%, 2.5%, 3% Tm-doped YLF samples match the literature rather well. As an example, a fluorescence lifetime of 16.85 ms is reported for a 3% Tm-doped YLF sample in [65], a value very close to our result (17 ms). On the other hand, we have measured a rather long fluorescence lifetime (16.3 ms) even for the 6% Tm-doped YLF (this data has been repeated many times for confirmation). We believe the long lifetime measured for this sample indicates that the crystal used in this work is of high quality with minimal level of impurities. Interestingly, high-purity Tm:YLF crystals with high optical quality is also attractive for the development of mid-IR optical cryocoolers and radiation balanced lasers [14]. Recently, an external quantum efficiency of 0.98 is measured for the $^3F_4$ decay, for 1% and 2% Tm-doped YLF crystals, along with background absorption values as low as 0.02-0.03% per cm [14]. As we will outline in our lasing experiments in Section 4, we have estimated the passive losses of our 6% Tm-doped sample as 0.05% per cm. Basically, passive loss level of the Tm:YLF crystals is an indirect indicator for the presence of impurities, which are known to reduce fluorescence lifetime and quantum efficiency. Our results suggest

Optics EXPRESS

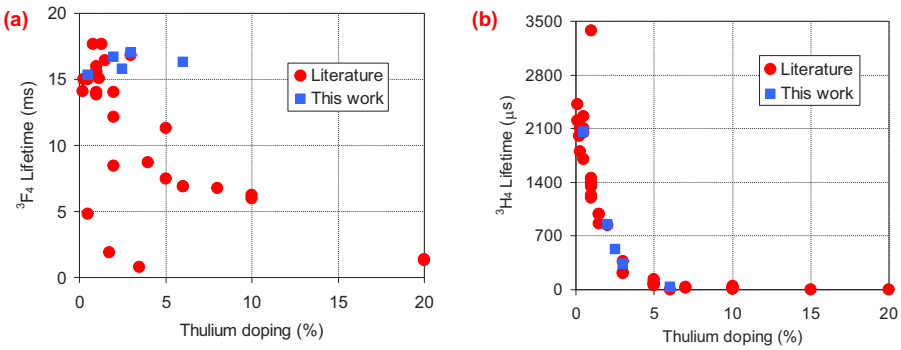

Fig. 5. Measured variation of Tm:YLF (a) $^3F_4$ level and (b) $^3H_4$ level room temperature fluorescence lifetime with thulium doping. The square blue markers are data taken in this work, whereas the circular red markers indicate earlier data in the literature.

that good quality Tm:YLF crystals could be grown even with doping levels as high as 6%, and detailed future work is required to confirm these initial findings.

Figure 5 (b) shows the literature data on the measured variation of the $^3H_4$ level fluorescence lifetime of Tm:YLF at room temperature, as a function of thulium doping [17,19,31,54,55,58,64,65,69–73]. We have measured the $^3H_4$ level lifetime as 1990 µs, 850 µs, 530 µs, 340 µs and 35 µs for the 0.5%, 2%, 2.5%, 3% and 6% Tm-doped YLF samples, respectively. As we can see from Fig. 5 (b), measured lifetime values for the $^3H_4$ transition is in good agreement with literature. As discussed earlier, the radiative lifetime of $^3H_4$ level is around 2 ms [64,69,73], and the reduction of fluorescence lifetime with doping is mostly due to two-for-one cross-relaxation process, which improves the lasing performance while lasing from the $^3F_4$ manifold [38,74].

Overall, for the 6% Tm-doped sample, the measured long fluorescence lifetime for the $^3F_4$ manifold suggests that it has low-level of impurities and low passive losses. Moreover, the measured short fluorescence lifetime of $^3H_4$ level shows the existence of a strong cross relaxation process. Both of these favors efficient lasing operating around 1.9 µm, as it will be discussed in the coming sections.

3.2. Emission cross-section measurements

Figure 6 shows the measured emission cross section of Tm:YLF at room-temperature for both of its E//a and E//c axes. The measured emission cross section (ECS) curves are in relatively good agreement with earlier reports in literature [26,28,55,75,76], and especially a quite good match (~ ±5%) is observed to the data presented by So et al. [26]. The E//c axis of Tm:YLF has four strong emission peaks centered around 1684 nm, 1745nm, 1832nm and 1880nm with emission cross section values of around 3.37×10^{-21} cm^2, 2.42×10^{-21} cm^2, 3.46×10^{-21} cm^2 and 3.54×10^{-21} cm^2, respectively. For E//a axis, the peaks are centered around 1684 nm, 1744nm, 1795nm, 1846nm, and 1908nm with strengths of 0.69×10^{-21} cm^2, 2.43×10^{-21} cm^2, 2.37×10^{-21} cm^2, 2.33×10^{-21} cm^2 and 2.35×10^{-21} cm^2, respectively. As we see, the peaks of E//c axis are stronger than E//a axis (around 1.5 fold). On the other hand, the emission peaks are located at different wavelengths for different axis, and optimization of lasing performance at different spectral regions might benefit from their mutual usage.

Due to the 3-level laser structure (especially on the short wavelength side of the spectrum), it is more beneficial to look at the gain cross section of Tm:YLF to better understand the potential laser performance. For this purpose, in Fig. 7 we show the calculated room-temperature gain cross section of Tm:YLF for inversion levels between 5% and 55% for both of its axes. For an easier comparison of the gain cross section in E//a and E//c axes, Fig. 8 shows them together in

Optics EXPRESS

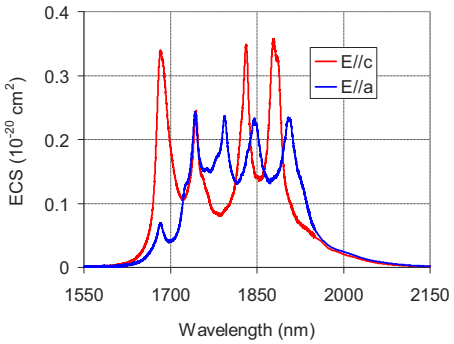

Fig. 6. Measured room-temperature emission cross section of Tm:YLF in E//a and E//c axes at room temperature for the $^3F_4 \rightarrow {}^3H_6$ transition.

one graph, at selected inversion levels between 15% and 100%. Note that, in Fig. 8, we present the data in logarithmic units for better visibility of the gain spectra at regions where the gain is rather small. Moreover, the long wavelength range is extended up to 2250 nm to see the gain behavior in this region.

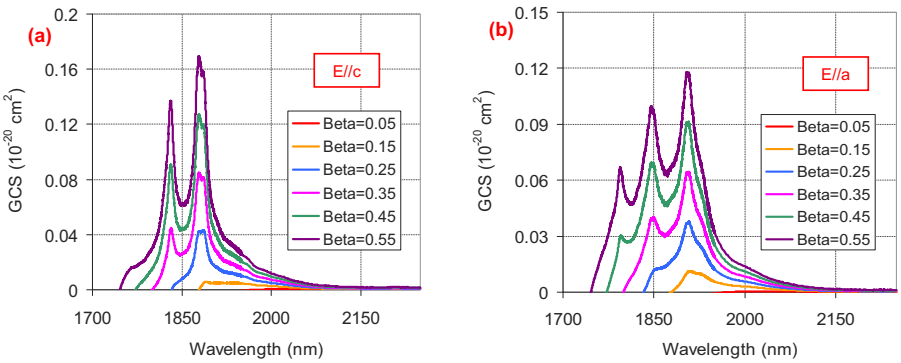

Fig. 7. Calculated room-temperature gain cross section (GCS) of Tm:YLF for the $^3F_4 \rightarrow {}^3H_6$ transition, for (a) E//c and (b) E//a axes for inversion levels between 5% and 55%.

We would like to underline several interesting points that could be observed from Figs. 7 and 8. First of all, as mentioned earlier, the peak gain cross section in E//c axis is stronger than E//a axis, making it the ideal candidate for laser development. Among the four emission peaks of the E//c axis (Fig. 6), only the two strong peaks around 1832nm and 1880nm possesses high gain due to the overlapping absorption band reducing gain in the short wavelength region. For the E//a axis, the gain peaks at 1846nm and 1908nm are rather strong. At high inversion levels, the 1795nm emission peak also becomes relatively visible. Note that, for both axes, the gain spectrum is relatively smooth at low inversion levels. Hence, ideally for ultrashort pulse generation and amplification with Tm:YLF, the inversion levels should be kept low for minimization of gain filtering effects (which contradicts with the need to get high inversion for high gain). As the inversion is increased, the dominant gain peaks (especially for E//c axis), will prevent usage of the full bandwidth. As an advantage, despite its lower overall gain, the E//a axis gain spectra is actually smoother and slightly broader. Looking at Fig. 8, we also see that, the E//a axis actually has higher gain for wavelengths above 1895nm, and also for the 1750-1815nm and 1840-1865nm intervals.

Optics EXPRESS

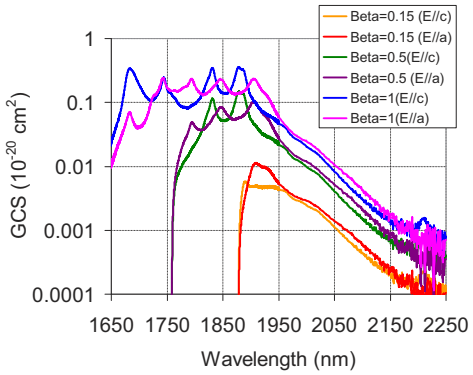

Fig. 8. Comparison of room-temperature gain cross section (GCS) of Tm:YLF in E//c and E//a axis for inversion levels of 15%, 50% and 100% for the $^3F_4 \rightarrow {}^3H_6$ transition. The small gain peak around 2200 nm is due to the $^3H_4 \rightarrow {}^3H_5$ transition.

4. Continuous-wave lasing results

We have started our Tm:YLF lasing experiments with multimode-diode pumping and in the first set of experiments data is taken using the 7 mm long 3% Tm-doped YLF crystal. Figure 9 (a) summarizes the measured continuous wave lasing performance of the diode pumped Tm:YLF laser using this crystal. Lasing has been investigated with output couplers with transmission in the 0.5-15% range. With the 0.5% OC, we have measured a lasing threshold of 0.2 W, and the laser produced 1.1 W of output power around 1997nm at an absorbed pump power of 2.7 W (incident power: 3.73 W, absorption: 73%). The slope efficiency with respect to incident and absorbed pump power were 34% and 47%, respectively. Note that, the absorption of the crystal at these fluences is below 60% in non-lasing case due to pump saturation, and via stimulated emission, the intracavity laser light balances the pump saturation and holds the absorption above 70% in lasing case.

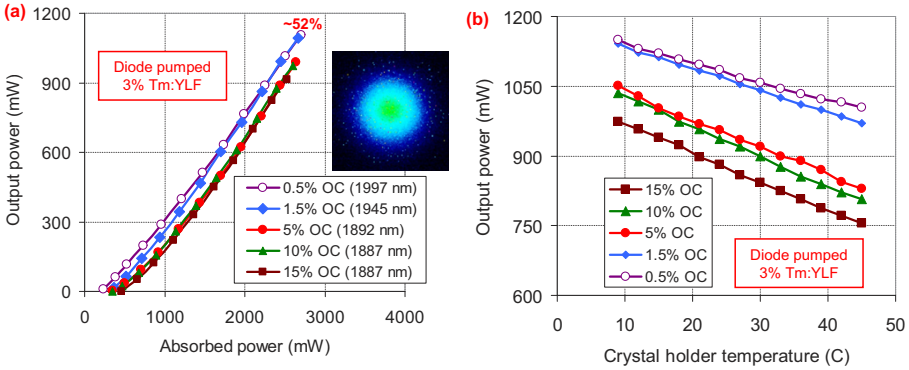

Fig. 9. (a) Measured cw efficiency curves for the multimode diode Tm:YLF laser under different output coupling. The data is taken using the 3% Tm-doped 7 mm long Tm:YLF crystal. For each OC, the free running laser wavelength is given in the legend. The laser gain peak shifts to shorter wavelengths at increased inversion levels (increased output coupling), which results in an observable blue shift in the measured free tuning laser wavelength. Inset shows sample near field beam profile. The data is taken at a crystal holder temperature of 15 °C. (b) Measured variation of cw laser performance with crystal holder temperature at different output coupling values. The data is taken at an incident pump power of 3.73 W.

Optics EXPRESS

A similar performance is achieved using a 1.5% transmitting output coupler, where we have measured a lasing threshold of 0.35W and obtained a cw power of 1.09 W around 1945nm at an absorbed pump power of 2.66 W. The slope efficiency with respect to absorbed pump power remained in the 50-52% range for output couplers with transmissions in the 1.5-15% interval. The laser output mode was symmetric and had a TEM_{00} profile despite usage of the multimode pump beam (inset in Fig. 9 (a), taken at 1 W output power level, both the near field and far field beam profiles showed a clean beam profile). Note that, for comparison, in our earlier studies, while lasing Cr:LiCAF lasers around 800 nm [77], or Yb:YLF lasers around 1020 nm [78] with similar multimode pumps, we have observed multimode laser output beams. We believe that in the case of Tm:YLF, due to the larger beam waist that is used, the Rayleigh range of the laser beam is longer, and a TEM_{00} beam could be obtained here (a TEM_{00} beam still provides a good mode matching to the multimode pump light). In Fig. 9, free running lasing wavelength for each output coupler is also given in the figure legend. As expected from the measured variation of gain spectra with inversion (Figs. 7, 8), the laser gain peak shifts to shorter wavelengths at increased inversion levels (increased output coupling ratios). Once the inversion is high enough, lasing around the 1880nm peak of E//c axis dominates.

We have also investigated the effect of thermal loading on the laser crystals by measuring the cw laser performance at various temperatures of the crystal holder and with different output couplers (Fig. 9 (b)). As we can see from Fig. 9 (b), for all the output couplers, as the crystal holder temperature is increased form 10 °C to 40 °C, the laser output power is reduced. Note that these are temperatures of crystal holder, and the estimated local temperatures inside the crystal is around 20 °C higher than the crystal holder temperature at 3 W absorbed pump power level. During the experiments, we have confirmed that, the reduction in output power is not due to reduced amount of pump absorption. Moreover, the fluorescence lifetime of Tm:YLF is also rather insensitive to temperature changes, and it cannot be the reason for the observed decrease. We believe that, the observed decrease in output power is due to the reduced gain cross section. At increased temperatures, the emission cross section decreases and absorption cross section increases, and both of these reduce the gain cross section of the laser material. The reduced gain cross section increases lasing threshold and lowers laser slope efficiency and overall one gets lower laser output powers at elevated temperatures (as an example see Fig. 11 in [74]). We also see that, the rate of laser power decrease with temperature is higher at larger output coupling (4 mW/°C at 0.5% OC, and at 6.2 mW/°C at 15% output coupling), because at high output coupling, one is more sensitive to changes in lasing threshold. Moreover, at high output coupling, the lasing wavelength is shorter and the variation of gain cross section with temperature is larger.

In the next step of lasing experiments, we have compared the Tm:YLF laser performance at different Tm-doping levels. Figure 10 shows the measured efficiency of the multimode-diode pumped Tm:YLF laser for the 2%, 3% and 6% Tm-doped YLF crystals at an output coupling of 1.5%. The best laser performance is obtained using the 4 mm long 6% Tm-doped YLF sample, where we have obtained up to 1.42 W of output power with 56% efficiency around 1955nm using 2.9 W of absorbed pump power (3.73 W incident, 78% absorption, lasing threshold: 0.2 W). For comparison, the slope efficiency is as low as 38% for the 10 mm long 2% Tm-doped sample. We believe that, the improved performance at higher doping levels is mostly due to the increased role of cross-relaxation process, as it was also clear from earlier lifetime measurements. We note that, some of the performance increase might be also due to the better mode-matching between the laser and pump modes since shorter crystal lengths are employed for highly-doped samples (4 mm in 7%, 7 mm in 3% and 10 mm in 2% doping).

Figure 10 also shows the performance of the 6% Tm-doped sample while being pumped by the Ti:Sapphire laser. Compared to multi-mode diode pumping, due to its better beam quality, pumping with Ti:Sapphire reduced the lasing threshold considerably and improved the laser slope

Optics EXPRESS

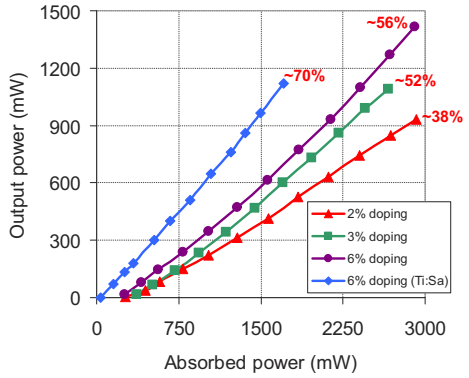

Fig. 10. Measured variation of cw laser performance with Tm-doping. The data is taken using the MMD pumped system and at an output coupling of 1.5%. For the 6% crystal, data taken with Ti:Sapphire pumping is also shown for comparison.

efficiency. To be more specific, while pumping with Ti:Sapphire laser, we have obtained 1.12 W of output power around 1951nm at an absorbed pump power of 1.71 W (incident pump power: 1.9 W, absorption:90%). A lasing threshold as low as 38 mW and a slope efficiency of 70% with respect to absorbed pump power has been achieved (compared to 200 mW lasing threshold and 56% slope efficiency obtained in multimode diode pumping). Note that, the Ti:Sapphire pump laser wavelength is tuned to 780 nm, where the absorption peak of the $^3H_6 \rightarrow {}^3H_4$ transition is located (absorption cross section (ACS) at 780 nm: $\sim 7 \times 10^{-21}$ cm^2 [79]. In comparison, the MMD diode is providing 792 nm pump light, where the ACS already reduces to around 5.5×10^{-21} cm^2 [79]. As a result, as it is already discussed in the experimental part, the absorption of the 6% Tm-doped Tm:YLF crystal is around 90% and 78% while pumping with Ti:Sapphire and MMD pump sources, respectively. Hence, the slope efficiency of the Tm:YLF laser with respect to incident pump power is also rather high (63%) while pumping with the Ti:Sapphire laser.

Motivated by this result, we have investigated the performance of the Tm:YLF laser under Ti:Sapphire pumping in more detail. Figure 11 (a) shows the measured lasing efficiency of the 6% Tm-doped crystal with output couplers with transmission in the range of 0.2-25% range. Using the 0.2% transmitting OC, we have measured a lasing threshold of only 18 mW, and obtained up to 0.83 W of output power around 1995nm at an absorbed pump power of 1.75 W. The slope efficiency with the 0.2% output coupler was as high as 48%, which clearly shows the low-loss nature of the laser crystal. Note that, at higher output coupling the slope efficiency increased to around 70% level. The slope efficiency obtained in this work (70%) is far above the Stokes limited slope efficiency (~780/1887≅41.3%) indicating a photon quantum efficiency of 1.69. To our knowledge, the slope efficiency and the photon quantum efficiency obtained in this work is one of the highest values reported for any Tm-based system in the literature [24,74,75,80,81].

To elaborate the observed performance a little deeper, we have used the measured variation of the laser slope efficiency with output coupler transmission to estimate the level of passive cavity losses (Caird analysis [82,83]). Investigating the measured performance (Fig. 11 (b)), we find that the round-trip passive loss of the system is only around 0.1 ± 0.05%. Note that, this corresponds to a loss of around 0.05% per cm and a quite high crystal figure of merit above 10000 for the 4 mm long 6% Tm-doped YLF crystal (assuming 0.06% of the round-trip loss comes from cavity mirrors, 0.01% loss per bounce, and 6 bounces in a cavity round-trip). As we will discuss in the next section in detail, we believe that the extremely low loss crystal used in

Optics EXPRESS

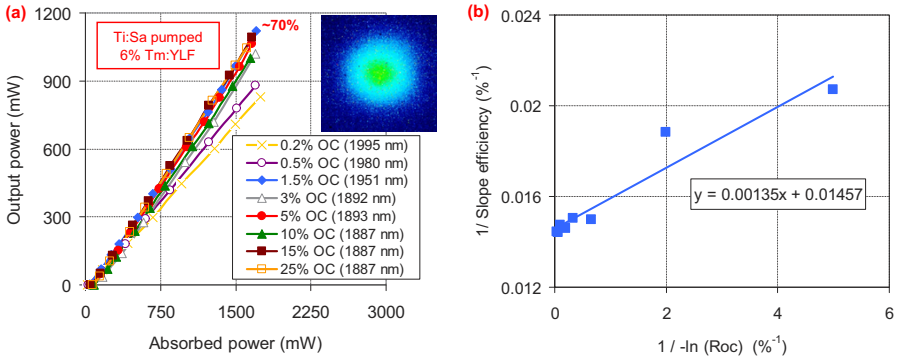

Fig. 11. (a) Measured cw efficiency curves for the Ti:Sapphire pumped Tm:YLF laser under different output coupling. The data is taken using the 6% Tm-doped 4 mm long Tm:YLF crystal. For each OC, the free running laser wavelength is given in the legend. The laser gain peak shifts to shorter wavelengths at increased inversion levels (increased output coupling), which results in an observable blue shift in the measured free tuning laser wavelength. (b) Measured variation of the inverse of the slope efficiency with the inverse of the output coupling percentage. Using Caird analysis, making a best-fit to the measured data (blue solid curve), we have estimated the round-trip passive cavity loss to be $0.1 \pm 0.05\%$. Roc: Reflectivity of the output coupler.

this study is one of the main reasons for the record tuning range achieved in this work (especially for the tuning range extension observed on the long wavelength side).

5. Laser tuning results

In this section, we would like to discuss our cw tuning results in detail. Figure 12 (a) shows the achieved cw tuning performance with the diode pumped system using output couplers in the 0.5-15% range. The data is taken with the 7 mm long 3% Tm-doped sample. Figure 12 (a) also includes calculated transmission of 1 m length of standard air. Figure 12 (b) shows the cw tuning results obtained from the Ti:Sapphire pumped system while employing the 4 mm long 6% Tm-doped YLF crystal, using output couplers with transmission in the 0.2-10% range. Estimated loss of the cavity high reflectors is also shown for TM polarized light in this graph (5 bounces on cavity high reflectors in one round-trip). The tuning behavior obtained is quite similar for both diode and Ti:Sapphire pumped systems. The Ti:Sapphire pump system enabled only a few nanometers extended tuning on the long wavelength side as its superior beam quality provides an advantage.

From Fig. 12, we see that, broader tuning ranges could be realized using low output coupling values (0.2-1.5% range). This is expected from the gain cross section curves that are presented earlier: as the output coupling and hence the net inversion/gain increases, the strong gain peaks of E//c axis centered around 1880nm and 1832nm becomes quite dominant, and prevents tuning the laser wavelength to the edges of the gain spectrum. Basically, as one tries to tune the laser to regions where the gain is low (towards the edge of emission spectrum), since the modulation depth of the birefringent filter is limited, the laser still prefers to operate in one of the main spectral peaks (1830nm or 1880nm line for the E//c axis of Tm:YLF). As an example, the Ti:Sapphire pumped system could only be operated near 1836nm, and in a smaller range near 1890nm using the 10% output coupler. On the other hand, at low output coupling, the gain spectrum is smoother and one can achieve broader tuning. As an example, using the 1.5% transmitting output coupler, the laser could be tuned from 1815nm to 2057nm in an almost smooth manner. Note that, the

Optics EXPRESS

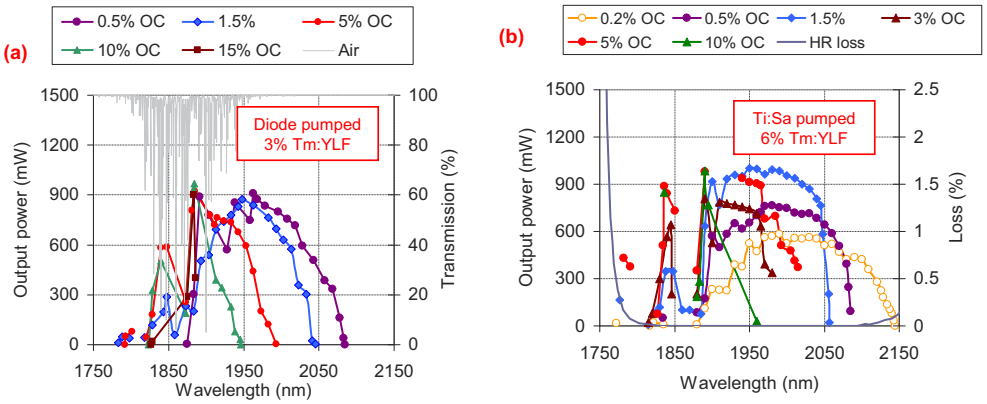

Fig. 12. Measured cw tuning curves for (a) diode pumped and (b) Ti:Sapphire pumped Tm:YLF laser under different output coupling. (a) Calculated transmission of 1 m length of standard air, and (b) estimated loss of the cavity high reflectors in one round-trip are also shown.

drop of power near 1860nm region is in good agreement with the GCS curves discussed earlier for the E//c axis.

On the long wavelength side, we have reached a cw lasing wavelength of 2057nm with 1.5% OC, 2085nm with 0.5% OC, and up to 2145 nm with the 0.2% OC. Basically, at this wavelength region there is ignorable level of overlap between the emission and absorption bands, and the system is effectively 4-level. While decreasing the losses via reducing the output coupling, lasing at longer wavelength could be accomplished in this long wavelength range, where the gain cross section is rather small. We would like to underline two important points here. First of all, the low level of cavity losses enables not only an overall net positive gain (despite low GCS), but it also provides a smoother gain profile in case of Tm:YLF, since the gain spectral shape heavily depends on inversion level. Of course, a smooth gain profile is very advantageous while trying to push the laser to operate at the edge of its gain spectra (above 2100 nm for the case of Tm:YLF). Secondly, the off-surface optical axis BRF used in this study enables higher sideband rejection compared to a regular BRF with an optical axis lying on its surface. Hence, some of the tuning range improvement observed in this study is due to the usage of BRFs with cut angles optimized for broadband tuning [39].

We believe that, our long wavelength tuning range is partly limited by the reduced gain cross section and partly limited due to increased losses of the cavity high-reflector set above 2150 nm (Fig. 12 (b)). Earlier literature reports tuning of Tm:YLF in the 1845-1935nm [42], 1879-1939.4 nm [43], 1860-1940nm [44], 1835-2010nm [36], 1831-2031nm [45], 1905-2067nm [28], and 2018-2096nm [37] regions(tuning results reported with the $^3F_4$ and $^3H_6$ transition of Tm:YLF). Hence, to the best of our knowledge, in this work we are presenting the first tuning of Tm:YLF above 2096nm, and our work extends the long wavelength tuning range of Tm:YLF up to 2145 nm (49 nm improvement compared to earlier results [34]). Lasing in the 2200-2460 nm range was earlier obtained while employing the $^3H_4$-$^3H_5$ transition of Tm:YLF [16], and the long wavelength edge of tuning achieved in this work (2145 nm), shows that due to phonon broadening there is only a small gap between these transitions. As a side note, looking at the gain cross section spectra of Tm:YLF (Fig. 8), we see that on the long wavelength side, the E//a axis of Tm:YLF has actually higher gain compared to the E//c configuration employed in this work. Hence, further improvement of laser performance could be feasible on the long wavelength side via employing the E//a axis.

Optics EXPRESS

On the short wavelength side, we could obtain smooth continuous tuning down to 1815nm. Moreover, to our surprise, we have also achieved tuning in the 1772-1801nm range using different output couplers, but with a small gap in lasing: lasing could not be achieved in the 1801-1815nm interval. We have also noticed that, while lasing in the 1772-1801nm interval, the laser polarization is not purely TM (p), but has a TE (s) component as well. We have realized that, while lasing in this short wavelength region, the laser cavity supported an arbitrary elliptical polarization state, and the polarization state was also observed to be varying with output coupling. Hence, while lasing in the 1772-1801nm, the TE (s) polarized part of the elliptically polarized intracavity beam gets reflected from the Brewster surfaces of the laser crystal and birefringent filter. As an example, using the 1.5% OC, we get around 26 mW from the output coupler, and on top of that we have measured a total leakage of 278 mW from other cavity reflections (only the output measured from the OC is reported in Fig. 12). We believe that, the laser works in this mode to utilize the gain peak of E//a axis around 1795nm (for this wavelength region, the gain of E//a axis is much higher than E//c axis, Fig. 8). Moreover, the coatings of the HR mirrors were limited below 1800nm for TM polarized light, and had a leakage loss of around 1% around 1765nm. The reflective coatings are usually better (broader) for TE polarized light, and hence lasing in this mixed polarization state could also have advantages for the laser in terms of minimizing total cavity losses. Based on these observations, we believe that, in future studies by employing crystals cut for operation in the E//a axis, and by using cavity high-reflector mirrors with reflectivity extending down to 1700nm, lasing of Tm:YLF systems could be extended below the 1772nm limit that we have observed in this study. Despite these shortcomings of this initial work, to the best of our knowledge, we are also reporting the lowest wavelength tuning limit observed in Tm:YLF so far (earlier shortest wavelength lasing report is 1831nm [53]).

In closing, we would like to present Fig. 13, which shows sample optical spectra from the achieved tuning behavior. Along the tuning range, we could achieve FWHM linewidths below 0.5 nm, and even below 0.25 nm in some of the regions. The overall tuning range (1772-2145 nm, 373 nm) we have demonstrated in this work significantly extends the earlier reports (1831-2096nm: 265 nm overall tuning). We believe that, the observed improvement in this work is partly due to the low-loss high FOM Tm:YLF crystal employed, and partly due to the benefits of usage of an off-surface optical axis birefringent filter for tuning, as it will be outlined in the Appendix section in detail.

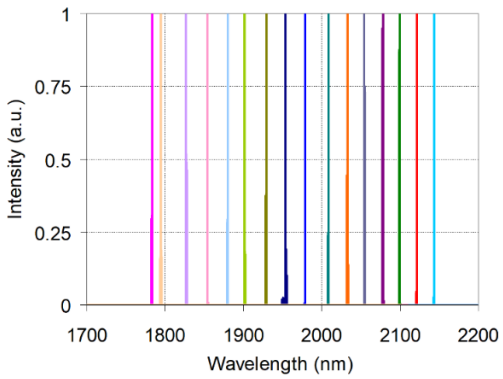

Fig. 13. Sample optical spectra from the cw Tm:YLF laser showing tunability in the 1772-2145 nm region.

Optics EXPRESS

6. Conclusions

In conclusion, we have presented detailed spectroscopic and lasing data mostly focusing on understanding of the tuning behavior of Tm:YLF lasers around 1900nm (for the $^3F_4$-$^3H_6$ transition). A record cw tuning range covering the 1772-2145 nm interval has been demonstrated, showing the great potential of Tm:YLF system for the development of ultrafast oscillators [7,32,84–87]. Detailed spectroscopic results and simulations of the birefringent filter are used to understand the observed performance. Further improvement in tuning behavior could possibly be obtained by employing the E//a axis of Tm:YLF, which has higher gain than the E//c axis, in both short and long wavelength edges. We have further estimated a passive loss level of 0.05% for the Tm:YLF crystal. The low loss crystal enables construction of high-Q laser cavities, which can store large intracavity power levels. Besides enabling ultrabroad tuning, such high-Q cavities has advantages for several other applications including intracavity second-harmonic generation [88] and ultralow timing jitter source development [89].

7. Appendix: Advantages of off-surface optical axis birefringent filters for tuning

Birefringent tuning plates are used in laser resonators for tuning of the output wavelength both in cw and mode-locked cases [90–95]. They can be inserted at Brewster's angle inside the laser cavity, and hence do not require anti-reflective coatings, and their passive losses could be quite low (ideally zero for TM polarized light). Important parameters of a BRF plate are modulation depth, side-band rejection strength, free-spectral range (FSR), transmission passband bandwidth (FWHM), and tuning rate (TR) . In this section, we would like to compare the filtering behavior of off-surface optical axis birefringent filters with typical on surface optical axis birefringent plates and discuss pros and cons of both approaches. Our focus will be on cw tuning of the Tm:YLF gain media, but the analysis is valid for other systems as well.

Figure 14 shows a schematic view of a BRF plate that is inserted at Brewster's angle into the laser cavity. The BRF plate has a thickness of t and σ is the angle between the optic axis and the surface normal of the BRF. Tuning of the laser wavelength is facilitated by rotation of the birefringent plate about an axis normal to the surface (corresponds to changing ρ in Fig. 14). In a typical/regular BRF; the optic axis lies on the surface, and $\sigma = 90°$. As discussed in earlier work, this particular choice ($\sigma = 90°$) which is convenient for fabrication, is not optimum for many applications. For BRFs made of crystal quartz, a cut angle of 25 degree ($\sigma = 25°$) has advantages in terms of the above mentioned filter parameters, and details of this choice could be found in our earlier work [39].

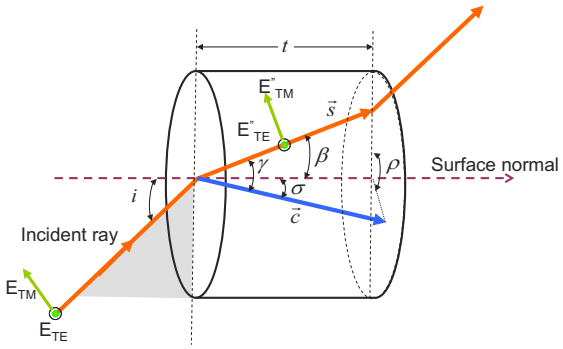

Fig. 14. Light beam incident on an off-surface optical axis birefringent plate that is placed at Brewster's angle inside a laser resonator [91]. σ: angle between the optic axis and the surface normal, c: optic axis, s: direction of beam propagation, i: incidence angle, β: internal Brewster's angle, ρ: rotation angle of the plate, t: thickness of the plate.

Optics EXPRESS

As a starting point, Fig. 15 shows the calculated transmission peaks of a standing wave Tm:YLF laser resonator containing a Brewster cut Tm:YLF crystal and a crystal quartz BRF plate inserted at Brewster's angle (such as in our cavity in Fig. 2 (a)). The calculation has been performed for two different cases of σ: (i) a regular on surface BRF (σ = 90°), and (ii) an off surface optical axis BRF with a diving angle of 25 degree (σ = 25°). For both cases, we have assumed a filter thickness of 2 mm. As the filter is rotated around an axis normal to the surface or as ρ is changed, at some resonant points we get transmission maxima for the selected central wavelength (2000nm in this case). The numbers (n) on the top of the graph shows different resonances of the filter (transmission peaks for 2000nm). The off-surface optical axis BRF has resonance transmission peaks at rotation angles of 35.1° (n = 1), 54.65° (n = 2), 71.15° (n = 3), 87.25° (n = 4), 104.6° (n = 5) and 125.9° (n = 6). The regular BRF has resonance transmission peaks at rotation angles (ρ) of 13.3° (n = 1), 38.8° (n = 2) and 58.85° (n = 3). Note that for ρ=0° and ρ=180°, the BRF has 100% transmission for all wavelengths (hence no filtering behavior) and these are not included. Moreover, for the regular BRF, the curve is symmetric around 90°, and transmission peaks in the 90-180° interval provide identical and hence only the 0-90° range is listed. For comparison, for the off-surface optical axis BRF, the curve is symmetric around 180° (hence the 180°-360° rotation provides a replica).

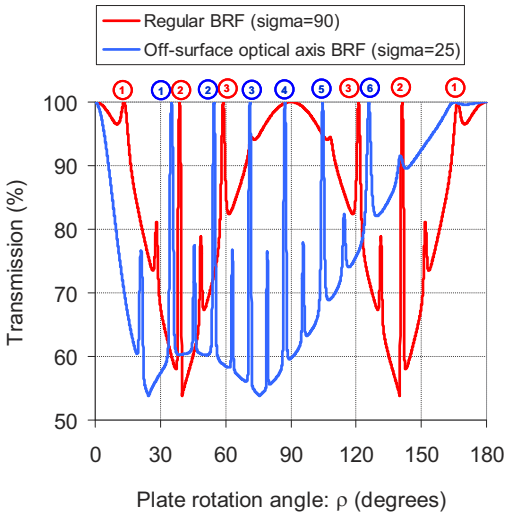

Fig. 15. Calculated variation of filter transmission as a function of BRF rotation angle (ρ) at the wavelength of 2000nm for a 2 mm thick BRF. The calculation has been performed for two cases: (i) for a regular on-surface optical axis BRF (σ=90°) and (ii) for an off-surface optical axis BRF with an optic axis orientation of 25°.

One can see from Fig. 15 that, for a given fixed plate thickness, the 25° cut off-surface optical axis BRF provides a larger set of resonances in comparison to a regular BRF (6 resonances compared to 3). Each of these resonances offer a different tuning behavior (possesses a different FSR, FWHM, tuning rate, etc. . .) and hence while using an off-surface optical axis BRF, one has larger set of available filter parameters to optimize the tuning behavior. To elaborate on this issue further, in Fig. 16, we plot the calculated filtering behavior of the BRFs around these different resonances for the 1500-2500 nm interval. Figure 16 (a) shows the calculation for the regular BRF around 13.3° (n = 1), 38.8° (n = 2) and 58.85° (n = 3). For the regular BRF, as we also see from Fig. 15, resonances around n = 1 and n = 3, provides rather small modulation depths of 8.5% and 22%, respectively. A filter with a small modulation (small side-band rejection) will have issues in pushing the wavelength of the laser to the edges of the gain curve, especially in cases

Optics EXPRESS

where the laser gain spectra is not smooth. Hence, tuning of the laser via these resonances will not provide the desired performance. In comparison, for n = 2, the BRF provides a rather large modulation depth of around 45%. On the other hand, as we see from Fig. 16 (a), the free spectral range of the regular BRF while tuning around this resonance is only 190 nm. For broadband gain media such as Tm:YLF with a tuning range close to 400 nm, such a short FSR will not provide the desired tuning behavior (might result in two-color lasing, which has advantageous for some applications [38]). Filter spectral range is inversely proportional with filter thickness t, and hence to get an FSR of around 400 nm, one needs a 1 mm thick crystal quartz BRF (such a BRF will have just one resonance n, around 38.8°). On the other hand, such thin regular BRFs has a very slow tuning rates, and could not accommodate a large enough free spectral range together with an acceptable modulation depth variation while tuning (as we will elaborate in a little bit more detail soon).

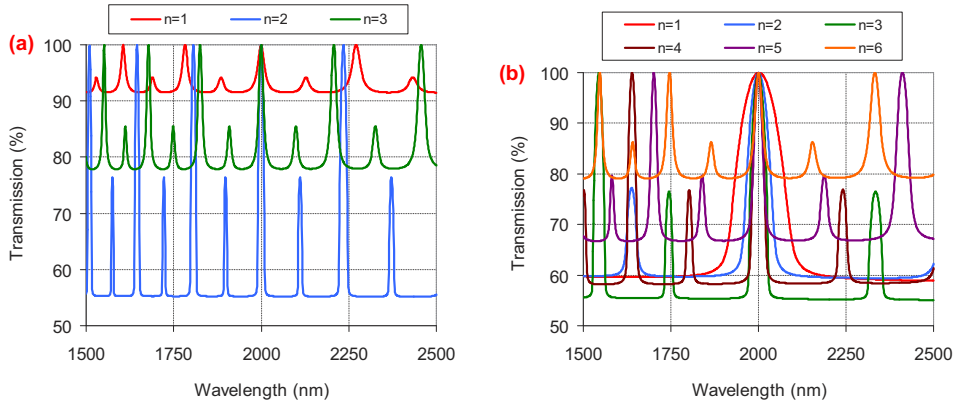

Fig. 16. Calculated transmission characteristics of a standing-wave Tm:YLF laser cavity for different orders of the BRF filter (different n values as show in Fig. 15). The calculation has been performed for two cases: (a) for a regular on-surface optical axis BRF (σ=90°) and (b) for an off-surface optical axis BRF with an optic axis orientation of 25°. The BRF filter thickness is taken as 2 mm in both cases.

For comparison, as we see from Fig. 16(b), for the 25° cut off-surface optical axis BRF, the modulation depth is reasonably high for many of the resonances. Moreover, the FSR range values are much larger compared to the regular BRF. Note also that the FWHM of the filter is different for different resonant orders, so one can tune this filter for tuning of cw lasers as well as femtosecond pulses as the FWHM is large enough to support sub-100-fs pulses [96]. The resonance around n = 3 (ρ = 71.15°) possesses the largest modulation depth (45%), and has a free-spectral range of around 600 nm and is quite suitable for tuning. Note that the FSR values specified here are average values, as the transmission maxima at the shorter wavelength side is closer to the main peak compared to the transmission maxima on the longer wavelength side.

We would like to finalize our discussion with Fig. 17, which compares the transmission characteristics of regular and off-surface optical axis BRF. Figure 17 shows the filtering characteristics of both BRFs around their optimum design point. For the regular BRF, a 1 mm thickness is chosen to achieve the desired 400 nm FSR. As we can see from Fig. 17 (a), the regular BRF has a very small tuning rate (10 nm per 1 degree of rotation), and one needs to scan a very large range with ρ (from 10° to 55°) to achieve tuning in the 1780-2150 nm region. On the other hand, as one rotates the filter, we see that the filter modulation depth varies significantly while tuning, and this will prevent broadband tuning of the Tm:YLF laser. For comparison, the 2 mm thick off-surface optical axis BRF with a 25° diving angle has a tuning rate of around 40 nm per degree of rotation, and hence a much narrower rotation range is required to scan the

Optics EXPRESS

1780-2150 nm region (rotation of ρ between 65 ° and 75° is sufficient). Note also from Fig. 17 (b) that, during this scan, the modulation depth of the filter remains above 40%, providing strong sideband rejection, enabling successful tuning of the Tm:YLF laser. In accordance with the simulations, in the tuning experiments with the off-surface optical axis BRF, the resonance peak around 71.15° (n = 3) provided the broadest tuning range in our experiments.

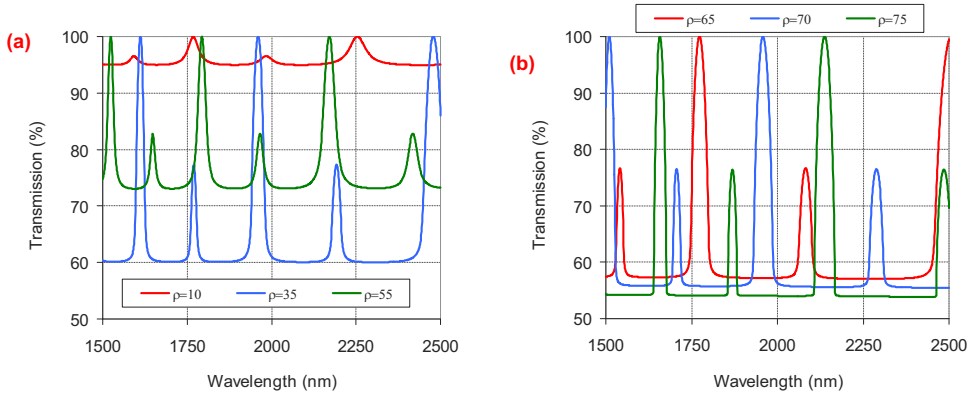

Fig. 17. Comparison of (a) regular and (b) off-surface optical axis BRF transmission characteristics in a standing-wave Tm:YLF laser cavity. For each case, tuning around the optimum order is shown: for n = 1 for the regular 1 mm thick BRF and for n = 3 for the 2 mm thick off-surface optical axis BRF with 25° diving angle.

Funding. Deutsche Forschungsgemeinschaft (390715994); European Research Council (609920).

Acknowledgements. UD acknowledge support from BAGEP Award of the Bilim Akademisi.

Disclosures. The authors declare no conflicts of interest.

Data Availability. Data underlying the results presented in this paper are not publicly available at this time but may be obtained from the authors upon reasonable request.

References

1. H. Fattahi, H. G. Barros, M. Gorjan, T. Nubbemeyer, B. Alsaif, C. Y. Teisset, M. Schultze, S. Prinz, M. Haefner, M. Ueffing, A. Alismail, L. Vamos, A. Schwarz, O. Pronin, J. Brons, X. T. Geng, G. Arisholm, M. Ciappina, V. S. Yakovlev, D. E. Kim, A. M. Azzeer, N. Karpowicz, D. Sutter, Z. Major, T. Metzger, and F. Krausz, "Third-generation femtosecond technology," Optica **1**(1), 45–63 (2014).
2. A. L. Calendron, J. Meier, M. Hemmer, L. E. Zapata, F. Reichert, H. Cankaya, D. N. Schimpf, Y. Hua, G. Q. Chang, A. Kalaydzhyan, A. Fallahi, N. H. Matlis, and F. X. Kärtner, "Laser system design for table-top X-ray light source," High Power Laser Sci. Eng. **6**, e12 (2018).
3. U. Demirbas, M. Kellert, J. Thesinga, Y. Hua, S. Reuter, M. Pergament, and F. X. Kärtner, "Highly efficient cryogenic Yb:YLF regenerative amplifier with 250 W average power," Opt. Lett. **46**(16), 3865–3868 (2021).
4. C. W. Rudy, M. J. F. Digonnet, R. L. Byer, C. W. Rudy, M. J. F. Digonnet, and R. L. Byer, "Advances in 2-μm Tm-doped mode-locked fiber lasers," Opt. Fiber Technol. **20**(6), 642–649 (2014).
5. Y. Zhao, Y. Zhao, L. Wang, W. Chen, W. Chen, Z. Pan, Y. Wang, P. Liu, X. Xu, Y. Liu, D. Shen, J. Zhang, M. Guina, X. Mateos, P. Loiko, Z. Wang, X. Xu, J. Xu, M. Mero, U. Griebner, and V. Petrov, "SESAM mode-locked Tm:$LuYO_3$ ceramic laser generating 54-fs pulses at 2048nm," Appl. Opt. **59**(33), 10493–10497 (2020).
6. J. W. Zhang, F. Schulze, K. F. Mak, V. Pervak, D. Bauer, D. Sutter, and O. Pronin, "High-Power, High-Efficiency Tm:YAG and Ho:YAG Thin-Disk Lasers," Laser Photonics Rev. **12**(3), 1700273 (2018).
7. F. Canbaz, I. Yorulmaz, and A. Sennaroglu, "Kerr-lens mode-locked 2.3-μm Tm^{3+}:YLF laser as a source of femtosecond pulses in the mid-infrared," Opt. Lett. **42**(19), 3964–3967 (2017).
8. F. Cornacchia, A. Toncelli, and M. Tonelli, "2-μm lasers with fluoride crystals: Research and development," Prog. Quantum Electron. **33**(2-4), 61–109 (2009).
9. C. W. Siders, T. Galvin, A. Erlandson, A. Bayramian, B. Reagan, E. Sistrunk, T. Spinka, and C. Haefner, "Wavelength Scaling of Laser Wakefield Acceleration for the EuPRAXIA Design Point," Instruments **3**(3), 44 (2019).
10. I. Tamer, B. A. Reagan, T. Galvin, J. Galbraith, E. Sistrunk, A. Church, G. Huete, H. Neurath, and T. Spinka, "Demonstration of a compact, multi-joule, diode-pumped Tm:YLF laser," Opt. Lett. **46**(20), 5096–5099 (2021).

Optics EXPRESS

11. A. P. Savikin, N. A. Egorov, N. G. Zakharov, O. N. Eremeĭkin, and V. V. Sharkov, "Investigating a thermal lens in a Tm:YLF crystal under intense diode pumping," J. Opt. Technol. **76**(11), 676–679 (2009).
12. U. Demirbas, M. Kellert, J. Thesinga, S. Reuter, F. X. Kärtner, and M. Pergament, "Advantages of YLF host over YAG in power scaling at cryogenic temperatures: direct comparison of Yb-doped systems," Opt. Mater. Express **12**(7), 2508 (2022).
13. B.-Q. Yao, P.-B. Meng, G. Li, Y.-L. Ju, and Y.-Z. Wang, "Comparison of Tm:YLF and Tm:YAP in thermal analysis and laser performance," J. Opt. Soc. Am. B **28**(8), 1866–1873 (2011).
14. S. Rostami, A. R. Albrecht, A. Volpi, M. P. Hehlen, M. Tonelli, and M. Sheik-Bahae, "Tm-doped crystals for mid-IR optical cryocoolers and radiation balanced lasers," Opt. Lett. **44**(6), 1419–1422 (2019).
15. S. So, J. I. MacKenzie, D. P. Shepherd, W. A. Clarkson, J. G. Betterton, and E. K. Gorton, "A power-scaling strategy for longitudinally diode-pumped Tm:YLF lasers," Appl. Phys. B **84**(3), 389–393 (2006).
16. J. F. Pinto and L. Esterowitz, "Tm^{3+}:YLF laser continuously tunable between 2.20 and 2.46 mm," Opt. Lett. **19**(12), 883–885 (1994).
17. V. Sudesh and J. A. Piper, "Spectroscopy, Modeling, and Laser Operation of Thulium Crystals at 2.3 μm," IEEE J. Quantum Electron. **36**(7), 879–884 (2000).
18. I. Yorulmaz and A. Sennaroglu, "Low-Threshold Diode-Pumped 2.3-μm Tm^{3+}:YLF Lasers," IEEE J. Sel. Top. Quantum Electron. **24**(5), 1–7 (2018).
19. P. Loiko, R. Soulard, L. Guillemot, G. Brasse, J.-L. Doualan, A. Braud, A. Tyazhev, A. Hideur, F. Druon, and P. Camy, "Efficient Tm:$LiYF_4$ Lasers at ~2.3 μ m: Effect of Energy-Transfer Upconversion," IEEE J. Quantum Electron. **55**(6), 1–12 (2019).
20. H. Huang, S. Wang, H. Chen, O. L. Antipov, S. S. Balabanov, and D. Shen, "High power simultaneous dual-wavelength CW and passively-Q-switched laser operation of LD pumped Tm:YLF at 1.9 and 2.3 μm," Opt. Express **27**(26), 38593–38601 (2019).
21. E. Kifle, P. Loiko, L. Guillemot, J.-L. Doualan, F. Starecki, A. Braud, T. Georges, J. Rouvillain, and P. Camy, "Watt-level diode-pumped thulium lasers around 2.3 μm," Appl. Opt. **59**(25), 7530–7539 (2020).
22. P. S. F. De Matos, N. U. Wetter, L. Gomes, I. M. Ranieri, and S. L. Baldochi, "A high power 2.3 μm Yb:Tm:YLF laser diode-pumped simultaneously at 685 and 960 nm," J. Opt. A: Pure Appl. Opt. **10**(10), 104009 (2008).
23. Y. F. Mao and L. Wang, "Study of high power Tm:YLF Innoslab wavelength-selected laser," Laser Phys. **29**(11), 115004 (2019).
24. A. Berrou, O. J. P Collett, D. Morris, and M. J. Daniel Esser, "Comparative study of high power Tm:YLF and Tm:LLF slab lasers in continuous wave regime," Opt. Express **26**(8), 10559–10572 (2018).
25. J. Li, S. H. Yang, A. Meissner, M. Hofer, and D. Hoffmann, "A 200 W INNOSLAB Tm:YLF laser," Laser Phys. Lett. **10**(5), 055002 (2013).
26. S. So, J. I. Mackenzie, D. P. Shepherd, and W. A. Clarkson, "High-power slab-based Tm:YLF laser for in-band pumping of Ho:YAG," in *Lasers and Applications in Science and Engineering* (SPIE, 2008), 6871, p. 68710R.
27. M. Schellhorn, S. Ngcobo, and C. Bollig, "High-power diode-pumped Tm:YLF slab laser," Appl. Phys. B **94**(2), 195–198 (2009).
28. A. Dergachev, J. H. Flint, Y. Isyanova, B. Pati, E. V Slobodtchikov, K. F. Wall, and P. F. Moulton, "Review of multipass slab laser systems," IEEE J. Sel. Top. Quantum Electron. **13**(3), 647–660 (2007).
29. E. R. Hale, I. Divliansky, and L. Glebov, "Passively Q switched dual channel Tm:YLF laser by intracavity spectral beam combination with volume Bragg gratings," Opt. Express **26**(13), 16670–16678 (2018).
30. A. Korenfeld, D. Sebbag, U. Ben-Ami, E. Shalom, G. Marcus, and S. Noach, "High pulse energy passive Q-switching of a diode-pumped Tm:YLF laser by Cr:ZnSe," Laser Phys. Lett. **12**(4), 045804 (2015).
31. M. Petros, J. Yu, U. N. Singh, B. M. Walsh, N. P. Barnes, J. C. Barnes, and M. Petros Jirong Yu, "300-mJ diode-pumped 1.9-um Tm:YLF laser," in *Proc. SPIE 4484, Lidar Remote Sensing for Industry and Environment Monitoring II* (SPIE, 2002), **4484**(9), 17–24.
32. A. Muti, F. Canbaz, M. Tonelli, J. E. Bae, V. Petrov, F. Rotermund, and A. Sennaroglu, "Graphene mode-locked operation of Tm^{3+}:$YLiF_4$ and Tm^{3+}:KY_3F_{10} lasers near 2.3 μm," Opt. Lett. **45**(3), 656–659 (2020).
33. H. J. Strauss, M. J. D. Esser, G. King, and L Maweza, "Tm:YLF slab wavelength-selected laser," Opt. Mater. Express **2**(8), 1165–1170 (2012).
34. P. A. Ketteridge, P. A. Budni, M. G. Knights, and E. P. Chicklis, "An All Solid-State 7 Watt CW, Tunable Tm:YLF Laser," in *Advanced Solid State Lasers (1997)*, Paper LS2 (Optica Publishing Group, 1997), p. LS2.
35. A. Dergachev, K. Wall, and P. F. Moulton, "A CW Side-Pumped Tm:YLF Laser," in *OSA TOPS Advanced Solid State Lasers*, M. E. Fermann and L. R. Marshall, eds. (OSA, 2002), **68**, pp. 343–346.
36. J. Šulc, H. Jelínková, P. Koranda, P. Černý, J. K. Jabczyński, W. Żendzian, J. Kwiatkowski, Y. Urata, and M. Higuchi, "Comparison of tunable lasers based on diode pumped Tm-doped crystals," in *Proceedings Volume 7141, 16th Polish-Slovak-Czech Optical Conference on Wave and Quantum Aspects of Contemporary Optics* (SPIE, 2008), 7141, pp. 98–104.
37. Y. Zhang, Y. Cai, B. Xu, Y. Yang, and Y. Hang, "Extending the wavelength tunability from 2.01 to 2.1 μm and simultaneous dual-wavelength operation at 2.05 and 2.3 μm in diode-pumped Tm:YLF lasers," J. Lumin. **218**, 116873 (2020).
38. E. Beyatli and U. Demirbas, "Widely tunable dual-wavelength operation of Tm:YLF, Tm:LuAG, and Tm:YAG lasers using off-surface optic axis birefringent filters," Appl. Opt. **57**(23), 6679 (2018).

Optics EXPRESS

39. U. Demirbas, "Off-surface optic axis birefringent filters for smooth tuning of broadband lasers," Appl. Opt. **56**(28), 7815–7825 (2017).
40. U. Demirbas, "Optimized birefringent filter design for broadly tunable multicolor laser operation of Nd-based lasers: Nd:YAG example," J. Opt. Soc. Am. B **35**(12), 2994 (2018).
41. J. Wei, X. Cao, P. Jin, J. Su, H. Lu, and K. Peng, "Diving angle optimization of BRF in a single-frequency continuous-wave wideband tunable titanium:sapphire laser," Opt. Express **29**(5), 6714 (2021).
42. J. K. Jabczynski, Gorajek W. Zendzian, J. Kwiatkowski, H. Jelínková, J. Šulc, and M. Němec, "High repetition rate, high peak power, diode pumped Tm:YLF laser," Laser Phys. Lett. **6**(2), 109–112 (2009).
43. J. K. Gorajek, W. Jabczyński, J. Zendzian, H. Kwiatkowski, J. Jelinkova, M. Sulc, and Nemec, "High repetition rate, tunable, Q-switched diode pumped Tm:YLF laser," Opto-Electronics Rev. **17**(4), 309–317 (2009).
44. O. N. Eremeikin, A. P. Savikin, K. Y. Pavlenko, and V. V Sharkov, "Diode-pumped tunable Tm : YLF laser for mid-infrared gas spectroscopy," Quantum Electron. **40**(6), 471–474 (2010).
45. E. Beyatli, "Low-cost multi-mode diode pumped Tm:YLF laser: Multi-color & Q-switching operations," Opt. Commun. **451**, 55–61 (2019).
46. U. Demirbas, J. Thesinga, M. Kellert, F. X. Kärtner, and M. Pergament, "Detailed investigation of absorption, emission and gain in Yb:YLF in the 78–300 K range," Opt. Mater. Express **11**(2), 250 (2021).
47. P. F. Moulton, "Spectroscopic and laser characteristics of Ti:Al_2O_3," J. Opt. Soc. Am. B **3**(1), 125–133 (1986).
48. D. Pugh-Thomas, B. M. Walsh, and M. C. Gupta, "Spectroscopy of $BeAl_2O_4$:Cr^{3+} with application to high-temperature sensing," Appl. Opt. **49**(15), 2891–2897 (2010).
49. D. E. McCumber, "Theory of phonon-terminated optical masers," Phys. Rev. **134**(2A), A299–A306 (1964).
50. D. E. McCumber, "Einstein relations connecting broadband emission and absorption spectra," Phys. Rev. **136**(4A), A954–A957 (1964).
51. M. L. Shand, J. C. Walling, and H. P. Jenssen, "Ground-State Absorption in the Lasing Wavelength Region of Alexandrite - Theory and Experiment," IEEE J. Quantum Electron. **18**(2), 167–169 (1982).
52. J. Korner, M. Kruger, J. Reiter, A. Munzer, J. Hein, and M. C. Kaluza, "Temperature dependent spectroscopic study of Yb^{+3}-doped $KG(WO_4)_2$, $KY(WO_4)_2$, $YAlO_3$ and $YLiF_4$ for laser applications," Opt. Mater. Express **10**(10), 2425–2438 (2020).
53. L. D. DeLoach, S. A. Payne, L. L. Chase, L. K. Smith, W. L. Kway, and W. F. Krupke, "Evaluation of Absorption and Emission Properties of Yb Doped Crystals for Laser Applications," IEEE J. Quantum Electron. **29**(4), 1179–1191 (1993).
54. E. P. Chicklis, J. Baer, M. Knights, and J. McCarthy, "XeF Pumped Tm:YLF Laser Scaling," (1984).
55. B. M. Walsh, N. P. Barnes, and B. Di Bartolo, "Branching ratios, cross sections, and radiative lifetimes of rare earth ions in solids: Application to Tm^{3+} and Ho^{3+} ions in LiYF4," J. Appl. Phys. **83**(5), 2772–2787 (1998).
56. S. A. Payne, L. L. Chase, L. K. Smith, W. L. Kway, and W. F. Krupke, "Infrared Cross-Section Measurements for Crystals Doped with Er^{3+}, Tm^{3+}, and Ho^{3+}," IEEE J. Quantum Electron. **28**(11), 2619–2630 (1992).
57. R. Soulard, M. Salhi, G. Brasse, P. Loiko, J.-L. Doualan, L. Guillemot, A. Braud, A. Tyazhev, A. Hideur, and P. Camy, "Laser operation of highly-doped Tm:$LiYF_4$ epitaxies: towards thin-disk lasers," Opt. Express **27**(6), 9287–9301 (2019).
58. A. Brenier, J. Rubin, R. Moncorge, and C. Pedrini, "Excited-state dynamics of the Tm^{3+} ions and $Tm^{3+} \rightarrow Ho^{3+}$ energy transfers in $LiYF_4$," J. Phys. **50**(12), 1463–1482 (1989).
59. J. Xiong, H. Peng, P. Hu, Y. Hang, and L. Zhang, "Optical characterization of Tm^{3+} in $LiYF_4$ and $LiLuF_4$ crystals," J. Phys. D: Appl. Phys. **43**(18), 185402 (2010).
60. V. Sudesh and E. M. Goldys, "Spectroscopic properties of thulium-doped crystalline materials including a novel host, $La_2Be_2O_5$: a comparative study," J. Opt. Soc. Am. B **17**(6), 1068–1076 (2000).
61. K. M. Dinndorf, *Energy transfer between thulium and holmium in laser hosts*, (Massachusetts Institute of Technology, 1993).
62. S. S. Li, H. P. Xia, L. Fu, Y. M. Dong, X. M. Gu, J. L. Zhang, D. J. Wang, Y. P. Zhang, H. C. Jiang, and B. J. Chen, "Optimum fluorescence emission around 1.8 μm for $LiYF_4$ single crystals of various Tm^{3+}-doping concentrations," Chinese Phys. B **23**(10), 107806 (2014).
63. J. W. Szela, *Planar waveguide lasers and spectroscopic study of upconversion solid-state materials*, (University of Southampton, 2015).
64. A. Braud, S. Girard, J. L. Doualan, and R. Moncorgé, "Spectroscopy and fluorescence dynamics of (Tm^{3+}, Tb^{3+}) and (Tm^{3+}, Eu^{3+}) doped $LiYF_4$ single crystals for 1.5-μm laser operation," IEEE J. Quantum Electron. **34**(11), 2246–2255 (1998).
65. M. Salhi, *Spectroscopie et caractérisation laser de cristaux massifs et de couches minces cristallines de fluorures dopés terres rares autour de 2 μm*, (Normandie Université, 2017).
66. B. M. Walsh, N. P. Barnes, M. Petros, J. Yu, and U. N. Singh, "Spectroscopy and modeling of solid state lanthanide lasers: Application to trivalent Tm^{3+} and Ho^{3+} in $YLiF_4$ and $LuLiF_4$," J. Appl. Phys. **95**(7), 3255–3271 (2004).
67. S. J. Beecher, J. W. Szela, and J. I. Mackenzie, "Towards an Experimentally Simple Procedure for the Determination of Energy Transfer Parameters in Gain Media," in *Advanced Solid State Lasers* (2013), p. AM4A.25.
68. U. Demirbas, J. Thesinga, M. Kellert, M. Pergament, and F. X. Kärtner, "Temperature and doping dependence of fluorescence lifetime in Yb:YLF (role of impurities)," Opt. Mater. **112**, 110792 (2021).

Optics EXPRESS

69. A. M. Tkachuk, I. K. Razumova, E. Y. Perlin, M. F. Joubert, and R. Moncorge, "Luminescence Self-Quenching in Tm^{3+}: YLF Crystals: II. The Luminescence Decay and Macrorates of Energy Transfer," Opt. Spectrosc. **90**(1), 78–88 (2001).
70. G. Armagan, A. M. Buoncristiani, A. T. Inge, and B. Di Bartolo, "Comparison of Spectroscopic Properties of Tm and Ho in YAG and YLF Crystals," in *Advanced Solid State Lasers (1991)*, Paper MIL14 (Optical Society of America, 1991), p. MIL14.
71. S. Wang, H. Huang, H. Chen, J. Xu, S. Liu, X. Liu, and D. Shen, "High efficiency nanosecond passively Q-switched 2.3 μm Tm:YLF laser using a ReSe2-based saturable output coupler," OSA Commun. **2**(5), 1676–1682 (2019).
72. I. Razumova and D. Mironov, "Spectral-luminescent properties of Tm:YLF crystal," J. Alloys Compd. **225**(1-2), 129–132 (1995).
73. G. La Rosa, *Spectroscopy of Tm^{3+} : YLF as a laser material for diode laser pumping*, (Massachusetts Institute of Technology, 1988).
74. E. Beyatli, B. Sumpf, G. Erbert, and U. Demirbas, "Efficient Tm:YAG and Tm:LuAG lasers pumped by 681 nm tapered diodes," Appl. Opt. **58**(11), 2973 (2019).
75. P. Loiko, J. M. Serres, X. Mateos, S. Tacchini, M. Tonelli, S. Veronesi, D. Parisi, A. Di Lieto, K. Yumashev, U. Griebner, and V. Petrov, "Comparative spectroscopic and thermo-optic study of Tm:$LiLnF_4$ (Ln = Y, Gd, and Lu) crystals for highly-efficient microchip lasers at ~2 μm," Opt. Mater. Express **7**(3), 844–854 (2017).
76. P. A. Budni, M. L. Lemons, J. R. Mosto, and E. P. Chicklis, "High-Power/High-Brightness Diode-Pumped 1.9 μm Thulium and Resonantly Pumped 2.1-μm holmium Lasers," IEEE J. Sel. Top. Quantum Electron. **6**(4), 629–635 (2000).
77. U. Demirbas, I. Baali, D. A. E. Acar, and A. Leitenstorfer, "Diode-pumped continuous-wave and femtosecond Cr:LiCAF lasers with high average power in the near infrared, visible and near ultraviolet," Opt. Express **23**(7), 8901 (2015).
78. U. Demirbas, J. Thesinga, M. Kellert, S. Reuter, M. Pergamnet, and F. X. Kärtner, "Semiconductor saturable absorber mirror mode-locked Yb:YLF laser with pulses of 40 fs," Opt. Lett. **47**(4), 933–936 (2022).
79. C. E. Aleshire, C. X. Yu, P. A. Reed, and T. Yee Fan, "Efficient cryogenic near-infrared Tm:YLF laser," Opt. Express **25**(12), 13408–13413 (2017).
80. Q. Na, C. Xu, Z. Huang, M. He, Z. Chen, T. Xu, L. Wang, P. Yan, Y. Li, S. Luo, and D. Fan, "High-power and high-efficiency short wavelength operation of a Tm:YLF laser at 1.83 μm," Opt. Lett. **44**(17), 4403–4406 (2019).
81. N. G. Zakharov, O. L. Antipov, A. P. Savikin, V. V Sharkov, O. N. Eremeikin, Y. N. Frolov, G. M. Mishchenko, and S. D. Velikanov, "Efficient emission at 1908nm in a diode-pumped Tm:YLF laser," Quantum Electron. **39**(5), 410–414 (2009).
82. J. A. Caird, S. A. Payne, P. R. Staver, A. J. Ramponi, L. L. Chase, and W. F. Krupke, "Quantum electronic properties of the $Na_3Ga_2Li_3F_{12}$:Cr^{3+} laser," IEEE J. Quantum Electron. **24**(6), 1077–1099 (1988).
83. A. Sennaroglu, "Classification of power-degrading mechanisms in an optically pumped four-level laser: an analytical approach," J. Opt. Soc. Am. B **36**(8), 2202–2209 (2019).
84. Q. Na, Z. Huang, M. He, Z. Chen, T. Xu, L. Wang, P. Yan, Y. Li, S. Luo, C. Xu, and D. Fan, "Watt-level passively mode-locked Tm:YLF laser at 1.83 μm," Opt. Express **27**(24), 35230–35237 (2019).
85. A. Tyazhev, R. Soulard, T. Godin, M. Paris, G. Brasse, J. L. Doualan, A. Braud, R. Moncorgé, M. Laroche, P. Camy, and A. Hideur, "Passively mode-locked diode-pumped Tm^{3+}:YLF laser emitting at 1.91 μm using a GaAs-based SESAM," Laser Phys. Lett. **15**(4), 045807 (2018).
86. R. Soulard, A. Tyazhev, J. L. Doualan, A. Braud, A. Hideur, M. Laroche, B. Xu, and P. Camy, "2.3 μm Tm^{3+}: YLF mode-locked laser," Opt. Lett. **42**(18), 3534–3536 (2017).
87. J. Mužík, M. Jelínek, D. Vyhlídal, and V. Kubeček, "2.6 W diode-pumped actively mode-locked Tm:YLF laser," Laser Phys. Lett. **12**(3), 035802 (2015).
88. U. Demirbas, "Cr:Colquiriite Lasers: Current status and challenges for further progress," Prog. Quantum Electron. **68**, 100227 (2019).
89. D. Li, U. Demirbas, A. Benedick, A. Sennaroglu, J. G. Fujimoto, and F. X. Kärtner, "Attosecond timing jitter pulse trains from semiconductor saturable absorber mode-locked Cr:LiSAF lasers," Opt. Express **20**(21), 23422 (2012).
90. S. M. Kobtsev and N. A. Sventsitskay, "Application of birefringent filters in continuous-wave tunable lasers: a review," Opt. Spectrosc. **73**(1), 114–123 (1992).
91. S. Lovold, P. F. Moulton, and D. K. Killinger, "Frequency Tuning Characteristics of a Q-Switched Co:MgF_2 Laser," IEEE J. Quantum Electron. **21**(3), 202–208 (1985).
92. A. L. Bloom, "Modes of a laser resonator containing tilted birefringent plates," J. Opt. Soc. Am. B **64**(4), 447–452 (1974).
93. S. Zhu, "Birefringent filter with tilted optic axis for tuning dye lasers: theory and design," Appl. Opt. **29**(3), 410–415 (1990).
94. K. Naganuma, G. Lenz, and E. P. Ippen, "Variable Bandwidth Birefringent Filter for Tunable Femtosecond Lasers," IEEE J. Quantum Electron. **28**(10), 2142–2150 (1992).
95. G. H. Li and Y. Li, "Tuning Sensitivity of Dye-Laser Birefringent Filters," Appl. Opt. **29**(24), 3462–3463 (1990).
96. U. Demirbas, J. Wang, G. S. Petrich, S. Nabanja, J. R. Birge, L. A. Kolodziejski, F. X. Kärtner, and J. G. Fujimoto, "100-nm tunable femtosecond Cr:LiSAF laser mode locked with a broadband saturable Bragg reflector," Appl. Opt. **56**(13), 3812 (2017).